Special Interest Group Meeting on Precision Engineering for Sustainability
Kern Microtechnik GmbH, Bavaria, Germany, October 2024
www.euspen.eu

Machining of cemented carbide components in the context of green hydrogen

Andreas Nestler, Andreas Schubert

Chemnitz University of Technology, Professorship Micromanufacturing Technology, Reichenhainer Straße 70, 09126 Chemnitz, Germany

andreas.nestler@mb.tu-chemnitz.de

Abstract
Sustainability in mechanical engineering often entails wear reduction. For this reason, there is an increasing use of hard materials like cemented carbides, which are difficult to machine. A prospective application in the context of green hydrogen are forming tools for a large-batch production of bipolar plates. Machining of the forming tools can be realised by micromilling. But, there is only little information about suitable strategies for micromilling of complex geometries in cemented carbides.
The investigations focus on different strategies for micromilling of a typical flow field geometry in cemented carbide using CVD diamond coated ball end mills. The specimens consist of 80% tungsten carbide particles with a size of 2.5 µm and 20% cobalt as binder. The results show that a high geometrical accuracy can be achieved combined with low surface roughness values for a feed motion in the direction of the flow field channels. These findings can contribute to a higher sustainability by precision engineering.

Keywords: Bipolar plate, Cemented carbide, Diamond, Forming tools, Micromilling

1. Introduction

The 7th Sustainable Development Goal (SDG) established by the United Nations aims for a wide access to affordable, reliable and clean energy. For the reduction of greenhouse gas emissions and the transition to renewable energies, hydrogen plays a crucial role. On the one hand, in times of electricity surplus energy can be converted and stored in hydrogen using electrolysers. On the other hand, hydrogen allows for a conversion in electrical energy by fuel cells. For both systems, a large number of bipolar plates is required. Consequently, their costs are very important with regard to high volumes. An inexpensive solution is represented by metallic bipolar plates. Metal forming of the sheets can be realised by deep drawing or hollow embossing rolling. To save weight and resources, a reduction of the sheet thickness is aimed for. Because of the low sheet thickness, tolerances and wear of the forming tools have to be very small. A high mechanical wear resistance can be achieved by the application of hard tool materials like cemented carbides, which typically consist of tungsten carbide (WC) particles and a cobalt binder. Further elements can be added to adjust the material properties. In general, cemented carbides are characterised by a high hardness, strength and Young's modulus. Furthermore, there is a good corrosion resistance.

However, manufacturing of cemented carbide forming tools is challenging. Electrical discharge machining (EDM) involves significant tensile residual stresses [1] and a recast layer impairing the wear resistance [2]. Moreover, for the generation of complex shapes by die sinking, specific form electrodes have to be manufactured. Last but not least, the removal of the detrimental surface layer, e.g. by grit blasting, entails an additional effort. In contrast, grinding allows for the generation of high-precision surfaces with compressive residual stresses [1]. But, because of the process kinematics, grinding is primarily suitable for machining of simple geometries like plane or cylindrical surfaces rather than complex shapes of embossing dies. An opportunity consists in micromilling. This process enables the precise creation of a wide variety of geometries combined with compressive residual stresses in the surface layer [3]. For machining of forming tools, milling is almost predestined because of high geometrical flexibility and beneficial surface properties. Nonetheless, the requirements concerning machining tool and milling cutters are very high. Because of the strongly abrasive effect of the hard WC particles in machining, diamond tools are applied. But, hard tungsten carbide particles represent a major challenge in machining.

For a high wear resistance, binderless diamond grades should be applied. In recent years, binderless nano-polycrystalline diamond tools were introduced. First tests in turning [4] and micromilling [5, 6] of cemented carbides with tools of this type show that high-quality surfaces with low roughness values and a long tool life can be obtained. However, such tools are expensive. In [7] the performance of different binderless diamond grades (monocrystalline diamond, CVD diamond (brazed tips) and CVD diamond coating with laser-treated cutting edges) were compared in face milling of cemented carbide. The surface roughness values obtained with the different diamond grades were in the same range. Concerning tool wear, CVD diamond coated tools performed best. Moreover, there have been different investigations in machining of cemented carbides with diamond coated ball end mills [8, 9]. The results show that long machining times are possible. The machining strategy can have a significant influence on tool life, as shown in [9] where machining of a taper and a rectangular pocket are compared. Nonetheless, there are nearly no investigations in the performance of the machining strategy for more complex geometries. Therefore, subsequently described research deals with the influence of the direction of feed motion and path planning in micromilling of a typical bipolar plate flow field geometry.

2. Experimental set-up and methodology

2.1. Material and specimens

The cemented carbide specimens used consist of about 80% WC particles with a size of 2.5 µm and 20% cobalt as binder. This material with the designation GB32 (produced by Boehlerit) is

assigned for forming tools and components affected by wear. The specimens had a size of approximately 20 mm × 25 mm × 5 mm. Both of the plane surfaces (20 mm × 25 mm) were ground to remove the sintered skin. On the one hand, this enabled a full-surface support of the specimens on the bearing area. On the other hand, there is a flat surface as starting basis for the generation of the microstructures. Their geometry is based on typical form elements of the flow field of fuel cells. Figure 1 shows the final geometry of the specimens after machining.

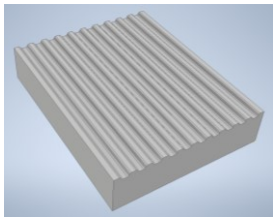

a) Overview

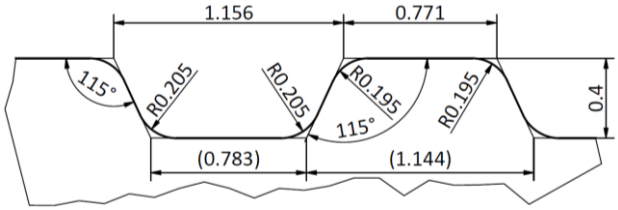

b) Geometry in detail with dimensions

Figure 1. Specimen geometry (after machining)

2.2. Experimental procedure

The experimental investigations were realised on a high precision machining centre of KERN type Nano Pyramid with an integrated dividing head. For the machining tests, the specimens were clamped on a baseplate using three dowel pins as stops and three eccentric fixture clamps consisting of a steel screw with an eccentric head and a hexagon brass washer. The clamping device was mounted on the dividing head via a zero-point clamping system with the interface EROWA ITS 100. This approach enabled tilting of the specimens to adjust the machining conditions. The experiments were carried out under compressed air supply to remove the chips and to cool the chip formation zone.

The generation of the channels was realised in three steps using CVD diamond end milling cutters. For rough machining of the channels, a double-edged ball end mill with a radius of 0.5 mm was applied. The direction of the feed motion was parallel to the channels. The channels should be premachined with an allowance of 30 µm on the bottom and the sides. However, because of the radius of the ball end mill, which is larger than the radii between the bottom and the sides, there remained a larger allowance, as shown in Figure 2. The cutting parameters for rough machining are summarised in Table 1.

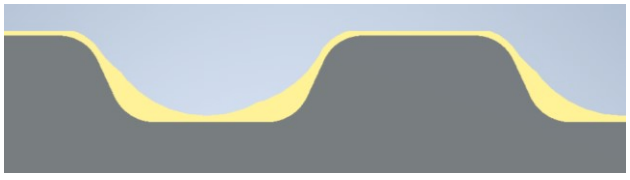

Figure 2. Detail of the specimen with allowance (yellow colour) after rough machining

Table 1. Cutting parameters for rough machining

Cutting parameter	Value	Unit
Spindle speed	40,000	min^{-1}
Feed per tooth	15	µm
Depth of cut	50	µm
Width of cut	100	µm

The next step was semifinishing by applying a double-edged ball end mill with a radius of 0.2 mm to achieve a uniform allowance of 20 µm (Figure 3).

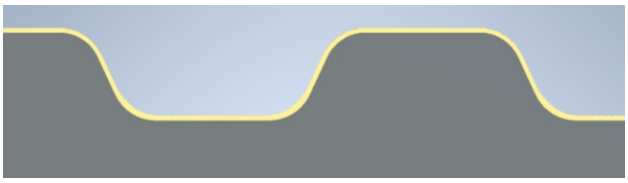

Figure 3. Detail of the specimen with allowance (yellow colour) after semifinishing

The channels were machined level by level in down-milling mode. The distance between the individual paths was about 30 µm along the contour resulting in a different spacing of the height levels. The spindle speed amounted to 40,000 min^{-1} and the feed per tooth was 3 µm.

For finish machining, which includes the surfaces of the channels and the bars, three different strategies were examined. The tool type was the same as for semifinishing, but for each of the finish machining strategies (one specimen per strategy) a new tool was used. Figure 4 shows SEM micrographs of this tool type.

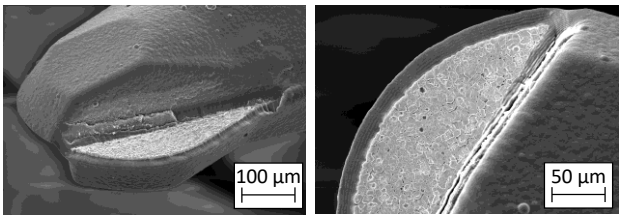

a) Overview b) Top view of rake face in detail

Figure 4. SEM micrographs of tool type for semifinishing and finish machining

On the rake faces, the diamond coating is removed to adjust an appropriate cutting edge condition. The coating thickness is almost 20 µm, which is much higher than the feed per tooth. The values for the feed per tooth and the spindle speed are the same as for semifinishing. Because of the higher proportion of plane surfaces (bottom of the channels and top faces of the bars), for all strategies used the specimens were inclined in the direction of the channels by 15°. This approach should avoid a contact between the specimen and the tool in the area, where the cutting speed is close to zero to reduce the tool wear and to achieve a high precision. The technical aim was a production of the channels within a tolerance band of ± 5 µm in relation to the target contour.

In the first strategy, the direction of feed motion was perpendicular to the direction of the channels. Machining was realised by down-miling and the distance of the paths amounted uniformly to 30 µm.

For the second strategy, the direction of feed motion corresponded to the direction of the channels. Machining started at the left front end. The single consecutive paths were directly adjacent to each other. The path spacing was 30 µm for the plane surfaces and 10 µm for the radii (along the contour) and the sides of the channels.

The third strategy was similar to the second one, but machining of the channels was realised for both sides (left and right) from top to bottom.

After machining tool wear and surface microstructure of the specimens were analysed by scanning electron microscopy using the secondary electron contrast. For roughness measurement of the specimens on the bar tops and the channel bottoms surface areas were detected by focus variation applying the optical

coordinate measuring system µCMM of Bruker Alicona. Measured data were analysed using the software MountainsMap from Digital Surf. The surface roughness depth *Rz* was determined in the longitudinal direction of the channels in the middle of the first, fifth, and ninth channel and bar, respectively. The total measured length amounted to 4 mm and the cut-off wavelength was 0.8 mm. Because of the low width of the channel bottoms and the bar tops, for the characterisation of the roughness across the direction of the channels the total height of the profile *Pt* was used. For each channel and bar considered (analogous to Rz), Pt was determined thrice (at the beginning, in the middle, and close to the end of the channels and bars, respectively). The evaluation length was 0.4 mm.

3. Results and discussion

3.1. Tool wear

To analyse the wear of the tools for finish machining after the experiments, SEM micrographs were used. Figure 5 shows images of the cutting edge and the rake face. Due to the similarity of wear of the two cutting edges, only the images of one cutting edge are represented.

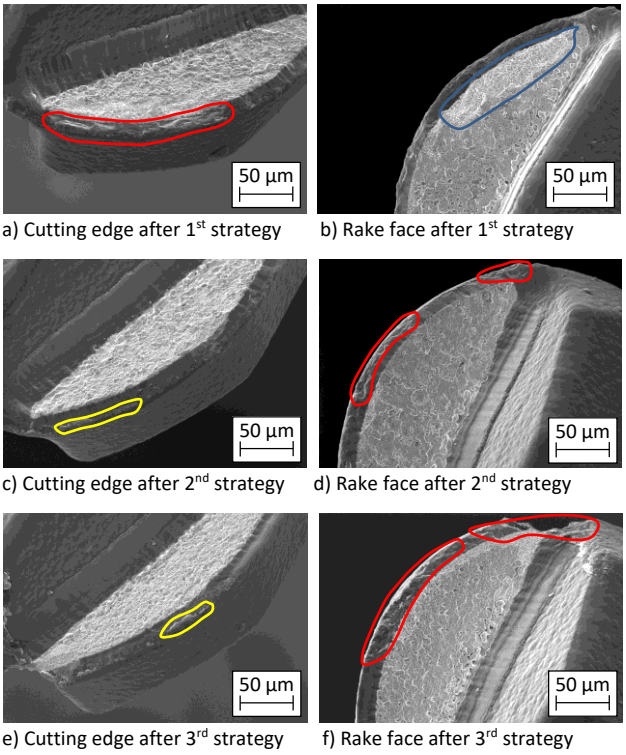

a) Cutting edge after 1st strategy b) Rake face after 1st strategy

c) Cutting edge after 2nd strategy d) Rake face after 2nd strategy

e) Cutting edge after 3rd strategy f) Rake face after 3rd strategy

Figure 5. SEM micrographs of the finish machining tools after the experiments (red: CVD diamond removal, blue: cemented carbide removal, yellow: material adherence)

After the first strategy with a feed motion in the direction perpendicular to the channels abrasive cutting edge wear can be clearly seen in a large area (red marking). Furthermore, there was material removal from the cemented carbide rake faces close to the cutting edge (blue marking). However, no severe wear occured, but compared to the other strategies tool wear was higher. This may be referred to the strongly changing cutting conditions when machining the channels. Furthermore, the inclination between the tool and the specimen was perpendicular to the direction of feed motion. This kinematics tends to stronger tool vibrations.

After the second strategy, the tool wear was significantly smaller. There was only a minor abrasive cutting edge wear (red marking). Furthermore, small material adherences are visible at the transition to the flank face.

The images of the tool used for the third strategy show a significant break-out (red marking, top) of the cutting edge at the centre of the tool. In addition, there is a medium abrasive cutting edge wear (red marking, left) combined with small material adherences (yellow marking). The reason for the break-out is not completely clear.

Concerning tool wear, the second strategy (adjacent paths from left to right) performed best. However, it has to be kept in mind that only one test was carried out for each strategy.

3.2. Surface properties

For a qualitative assessment of the surface microstucture micrographs taken by SEM were analysed. Figure 6 shows an overview of a part of the channel and the bar top (left side) and a detail of the channel bottom (right side) for all strategies tested.

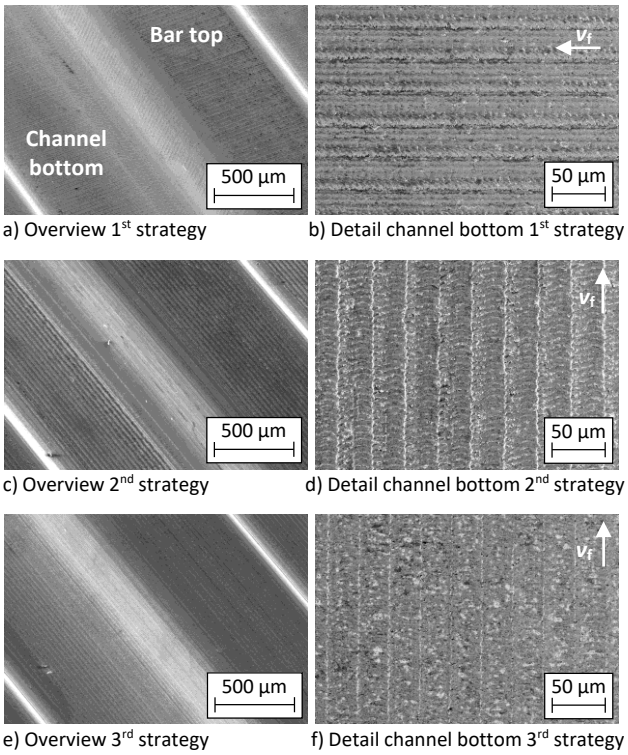

a) Overview 1st strategy b) Detail channel bottom 1st strategy

c) Overview 2nd strategy d) Detail channel bottom 2nd strategy

e) Overview 3rd strategy f) Detail channel bottom 3rd strategy

Figure 6. SEM micrographs of the specimens (v_f corresponds to feed motion referring to the tool)

For all strategies the feed marks can be clearly seen on the bar top and the channel bottom. On these surfaces, the spacing of the feed marks is uniformely about 30 µm. The surfaces generated by the first strategy are characterised by feed marks which are perpendicular to the channels. For the second and the third strategy, the direction of the feed marks corresponds to the orientation of the channels. The SEM micrograph of the specimen machined with the third strategy shows a lower spacing of the feed marks in the area between the channel bottom and the bar top (includes transition radii and side of channel). This corresponds to the reduced distance between the single paths in machining. However, for the second strategy the surface in this area does not exhibit clear feed marks. The surface seems to be smeared. This may be referred to the material adherence on the ball end mill (see Figure 5). The distance of the surface microstructures in the direction of feed motion resulting from the feed ist primarily visible for plane surfaces generated with the second strategy. However, for this case the spacing corresponds to the feed (not the feed per tooth). This indicates that the surface was created by only one cutting edge. Probably, there was an axial displacement between the two cutting edges.

The surface roughness was characterised by profile related parameters. Figure 7 shows the mean values and the scattering. The error bars indicate the range from the lowest to the highest measured values. The bars for *Rz* (green) represent the mean values out of six measured values (three from the channels and three from the bars). For *Pt*, the mean values were calculated from 18 individual values.

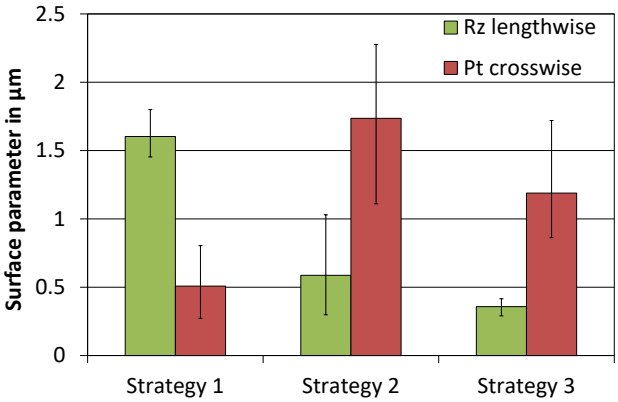

Figure 7. Surface parameters for the channel bottoms and the bar tops

For the first strategy with a feed motion perpendicular to the channels, the roughness values in the longitudinal direction are much higher than the values determined across. After applying the second or the third strategy, the relationship of the surface values is reversed. This can be explained by the changed direction of feed motion. The resulting kinematical roughness perpendicular to the direction of feed motion is reflected in these values. However, the calculated kinematical roughness amounts to about 0.6 µm for *Rz*. Because of slight deviations with regard to the positioning of the machine axes and the inhomogeneous material separation during machining the measured values are higher. The second strategy led for both directions to the highest mean values. This can be explained by an increase in the roughness values with cutting length. Maybe material adhesion on the tool and smearing on the surface increased. Concering the aim to generate surfaces with low roughness values, the third strategy performed best.

Another important aspect are the deviations from the nominal contour. Figure 8 shows the deviations of the contour in the middle of the fifth channel.

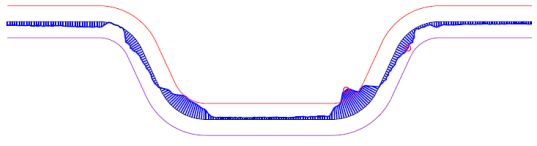

a) First strategy

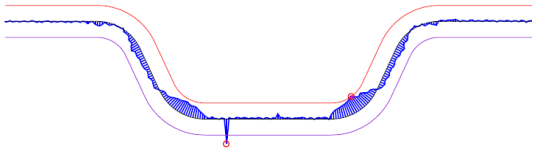

b) Second strategy

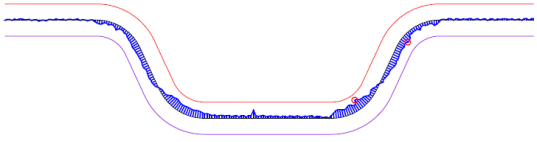

c) Third strategy

Figure 8. Contour of the channel (**black**: nominal contour, **red**: upper limit of tolerance band (+ 5 µm), **violet**: lower limit of tolerance band (- 5 µm), **blue**: deviation of measured contour)

In general, at the transition radii between the bottom and the sides of the channels, there remained a material allowance. It can be ascribed to the tool radius, which is only slightly smaller than the radius of the contour resulting in a stronger deflection of the ball end mill. This effect was most pronounced for the first strategy, characterised by the change of the direction of feed motion in the areas of the transition radius. The regions where the material removal led to an oversize of the channels may be referred to the NC programme. For a compensation of tool deflection and tool wear the radius value of the tools was reduced by 2 µm. Comparing the contour accuracy of the channels, the third strategy performed best.

4. Summary and conclusions

Investigations in micromilling of geometries which are typical for bipolar plate flow fields are carried out using cemented carbide specimens and CVD diamond coated ball end mills with a radius of 0.2 mm. Different machining strategies concerning he direction of feed motion and path planning are applied. The results show that a higher contour accuracy can be gained with a feed motion in the direction of the channels. In general, for a path spacing of 30 µm mean surface values (*Rz*, *Pt*) are smaller than 2 µm. The comparably regular surface profile perpendicular to the direction of feed motion indicates that a reduction of the roughness values can be achieved by a decreased path spacing. For a high contour accuracy, the radius of the ball end mill should be smaller than the transition radii between the channel bottom and the sides to reduce tool deflection. Each specimen of the size 20 mm × 25 mm is machined with only one tool for finishing. However, for micromilling of larger surfaces tool wear should be decreased.

Acknowledgements

European Union

Europe funds Saxony.
EFRE
European Regional Development Fund

This project is co-financed from tax revenues on the basis of the budget adopted by the Saxon State Parliament.

References

[1] Merklein M, Andreas K and Engel U 2011 *Procedia Eng.* **19** 252-7
[2] Bonny K, De Baets P, Ost W, Vleugels J, Huang S, Lauwers B and Liu W 2009 *Wear* **266** 84-95
[3] Okada M, Shinya M, Kondo A, Watanabe H, Sasaki T, Miura T and Otso M 2021 *J. Manuf. Process.* **61** 83-99
[4] Uhlmann E, Polte J, Hocke T and Polte C 2024 *Proceedings of euspen's 24th ICE* (Dublin, IE, 10-14 June 2024) 339-40
[5] Shimada H, Yano K and Kanada Y 2014 *Sei Tech. Rev.* **79** 86-90
[6] Uhlmann E, Polte M, Hocke T, Polte C and Polte J 2023 *Proceedings of euspen's 23rd ICE* (Copenhagen, DK, 12-16 June 2023) 493-94
[7] Nestler A and Schubert A 2021 *MM Sci. J. Special Issue HSM 2021 16th International Conference on High Speed Machining (Darmstadt, Germany, 26-27 October 2021)* 5038-45
[8] Silva EL, Pratas S, Neto MA, Fernandes CM, Figueiredo D and Silva RF 2021 *Mater.* **14** 3333
[9] Suwa H, Sakamoto S, Nagata M, Tezuka K and Samukawa T 2020 *Int. J. Autom. Technol.* **14** 1 18-25